

# Enhancing the absorption figure of merit on solution-based CuO thin films by Ni doping

Nguyen Van Loi<sup>a</sup>, La Thi Ngoc Mai<sup>b</sup>, Nguyen Hoang Luong<sup>b,c</sup>, Bui Nguyen Quoc Trinh<sup>b,d,\*</sup>

<sup>a</sup> Faculty of Physics, University of Science, Vietnam National University, Hanoi, 334 Nguyen Trai, Thanh Xuan, Hanoi, Viet Nam

<sup>b</sup> Nanotechnology Program, Faculty of Advanced Technology and Engineering, Vietnam Japan University, Vietnam National University, Hanoi, Luu Huu Phuoc, Nam Tu Liem, Hanoi, Viet Nam

<sup>c</sup> Nano and Energy Center, University of Science, Vietnam National University, Hanoi, 334 Nguyen Trai, Thanh Xuan, Hanoi, Viet Nam

<sup>d</sup> Key Laboratory for Micro-Nano Technology, University of Engineering and Technology, Vietnam National University, Hanoi, 144 Xuan Thuy, Cau Giay, Hanoi, Viet Nam

## ARTICLE INFO

### Keywords:

CuO  
Ni doping  
Oxide semiconductor  
Absorption length  
Absorption figure of merit

## ABSTRACT

We evaluated an absorbance effectiveness on the solar spectrum using an absorption figure of merit (*a*-FOM) for the conducting thin films. In particular, Ni-doped and un-doped CuO thin films were deposited by a facile and sustainable solution-processed synthesis, whose Ni doping concentration was varied to be 0.2, 0.6, 1, 2, 3, 4 wt%. We observed a change of smooth surface to an appearance of nanoparticles by Ni doping, which supported to form of a plasmonic mechanism for improving the light capture and retention. The absorption of long wavelengths was improved and extended to the near-infrared range. That is, the bandgap energy decreased from 2.10 to 1.88 eV with Ni doping. Also, we found that the absorption length decreased from 99.93 nm to 63.80 nm as the Ni doping increased. In addition, the CuO-based film with 4 wt% Ni doping showed a maximal value of *a*-FOM as high as  $30.88 \Omega^{-1} \text{cm}^{-1}$ , corresponding to a resistance of  $2.07 \text{ M}\Omega/\text{sq}$  and an absorption length of 63.80 nm. Our finding suggested that Ni-doped CuO thin films can be considered as an excellent selection of absorbent conductive oxide layers for application in optoelectronic devices and solar cell systems.

## 1. Introduction

Thin film materials are increasingly possessing exotic advances in the field of photovoltaic and optoelectronic applications, which play a role in highly absorbing materials like amorphous silicon (a-Si) [1] and GaAs [2]. The optical and electrical characteristics of films are two critical factors in evaluating the performance of photovoltaic and electronic devices, in order to tradeoff between the film quality and the cost-effective requirement. Several groups have judged the effectiveness of transparent conductive films in the relationship between the transmittance and the electrical resistance using a figure of merit (*FOM*), for instance, Yu et al. [3] prepared the transparent SnO<sub>2</sub>/Ag/SnO<sub>2</sub> films on glass substrates by sputtering technique. They obtained the sheet resistance of  $9.67 \Omega/\text{sq}$  and the average transmittance of 94.8%; the maximum value of the figure of merit of  $6 \times 10^{-2} \Omega^{-1}$ . In addition, Kim et al. [4] reported the influence of Al doping on the ZnO film (AZO) and produced transparent AZO/Ag/AZO multilayers. They found that the

optimum transmittance was about 93% at 550 nm, and the sheet resistance increased from  $3.86$  to  $4.47 \Omega/\text{sq}$  when the AZO film thickness increased from 9 to 45 nm. The thickness variation greatly affected the figure of merit, and its highest value was  $99.9 \times 10^{-3} \Omega^{-1}$ . Velusamy et al. [5] investigated the temperature effect on the optical property of In<sub>2</sub>O<sub>3</sub> films deposited by the electron beam evaporation technique. They pointed out that the bandgap energy was ranged from 3.67 to 3.85 eV. Particularly, the highest figure of merit of  $3.24 \times 10^3 \Omega^{-1} \text{ cm}^{-1}$  was obtained for the film annealed at 500 °C. The optical and electrical quality of NiO films with Pb-doping and (Ir, Pb) co-doping was also evaluated using the figure of merit. The films behaved the transparency of only 45–75%, corresponding to a decrease in sheet resistance from  $13 \times 10^4$  to  $6 \times 10^4 \Omega/\text{sq}$  for the Pb doping of 2%. The figure of merit of NiO: (1% Ir + 2% Pb) was as high as  $1.35 \times 10^{-7} \Omega^{-1}$  [6]. Cho et al. [7] determined *FOM* parameter for the CuO film deposited by sputtering at several growth temperatures. These authors obtained the highest figure of merit of  $0.17 \Omega^{-1} \text{ cm}^{-1}$  for the film grown at 300 °C with an optical

\* Corresponding author. Nanotechnology Program, Faculty of Advanced Technology and Engineering, Vietnam Japan University, Vietnam National University, Hanoi, Luu Huu Phuoc, Nam Tu Liem, Hanoi, Viet Nam.

E-mail address: [trinhbnq@vnu.edu.vn](mailto:trinhbnq@vnu.edu.vn) (B. Nguyen Quoc Trinh).

transmittance of 62.9% and the film mobility of  $6.6 \text{ cm}^2 \text{V}^{-1} \text{s}^{-1}$ . It is noted that the unit of FOM can be  $\Omega^{-1}$  or  $\Omega^{-1} \text{cm}^{-1}$ , depending on the use of sheet resistance or electrical resistivity for calculation, respectively. However, the above researches tried to optimize the transmittance and electrical conductivity of the transparent films by doping or creating multiple layers with high transmittance, but did not focus on developing absorption conductive thin films. To our best knowledge, no group has investigated the relationship between the electrical conductivity and the optical absorption characteristics by comparing the absorption efficiency to the solar spectrum. Therefore, we selected CuO-based films to deepen the absorption efficiency normalized with solar energy.

The CuO oxide semiconductor is well-known as a p-type component for photonic devices owing to its high light-harvesting, high intrinsic carrier concentration, and low heat emission. Recently, CuO nanostructure with a bandgap ranging from 1.2 to 1.9 eV [8] has been developed as a potential candidate of anode interlayers for the organic solar cells [9], the selective absorbers [10], and the photocatalysis [11]. The intriguing features of CuO have been an attractive topic of numerous attempts to reform them. In order to enhance the CuO quality, or even to develop a novel semiconductor material, the typical doping elements have been introduced. Up to the present, a lot of studies evidenced that transitional metals like Zn [12], Ni [13], Co [14] play an important role in CuO films to modify derivable properties. Nickel is one of the transitional metals that can be doped in the CuO base to extend its properties, and the radius of Ni ions (69 p.m.) is close to that of Cu ions (73 p.m.), which make the doping process become more effective. On the other hand, NiO has a wide bandgap ( $E_g = 3.5\text{--}4.0 \text{ eV}$ ) [15], work function ( $\sim 5.0 \text{ eV}$ ) [16], and high dielectric constant ( $10^3\text{--}10^4$ ) [17]. A combination between a narrow bandgap material like CuO and wide bandgap material like NiO could generate many exotic features for thin film development.

In this work, therefore, we represent the doping effect of the Ni transitional metal on the properties of CuO-based films deposited on glass substrates using a spin-coating method. Our aim was to elucidate

the role of Ni as a dopant on how to adjust the bandgap energy and the film resistivity. Interestingly, we proposed originally a new concept of absorption figure of merit (called as *a*-FOM) from calculating the absorption length to evaluate the absorption effectiveness of p-type conductive oxide films in relation to the solar spectrum.

## 2. Experimental details

### 2.1. Thin-film fabrication

Ni-doped and un-doped CuO thin films were deposited onto glass substrates at room temperature by a solution process. Fig. 1 shows a schematic drawing of the fabrication process with four stages used to obtain the films. In the stage A, the precursor of copper (II) acetate monohydrate,  $\text{Cu}(\text{CH}_3\text{COO})_2 \cdot \text{H}_2\text{O}$  was dissolved in ethanol solvent and monoethanolamine (MEA) was added into the solution as a stabilizer. The concentration of the precursor was controlled at 0.25 M and the molar ratio between the  $\text{Cu}^{2+}$  solution and MEA was kept at 1 : 2. For the Ni doping process, the various ratio of nickel acetate tetrahydrate,  $\text{Ni}(\text{CH}_3\text{COO})_2 \cdot 4\text{H}_2\text{O}$  was exactly adjusted from 0.2, 0.6, 1, 2, 3 to 4 wt% in the  $\text{Cu}^{2+}$  solution. The precursor solution was mixed with a magnetic stirrer at 75 °C for 60 min to ensure uniformity of solution and to form molecular bonds between nickel and copper ions. Here, the temperature of precursor formation is slightly lower than the boiling point of ethanol at 78 °C, in order to avoid rapid evaporation. For this stage, the solution is reacted in a closed system, i.e. completely sealed to limit the evaporation of ethanol from escaping. Moreover, the use of a magnetic stirrer ensures that the solution is continuously stirred, increasing contact between the solvent and the surrounding air. By combining these factors, solvent evaporation can be well controlled during the reaction, allowing the desired conditions for the chemistry to take place while minimizing solvent loss. In the stage B, glass substrates were ultrasonically cleaned with acetone, ethanol and then rinsed with deionized (DI) water to remove any organic contaminants. Next, in the stage C, the films were

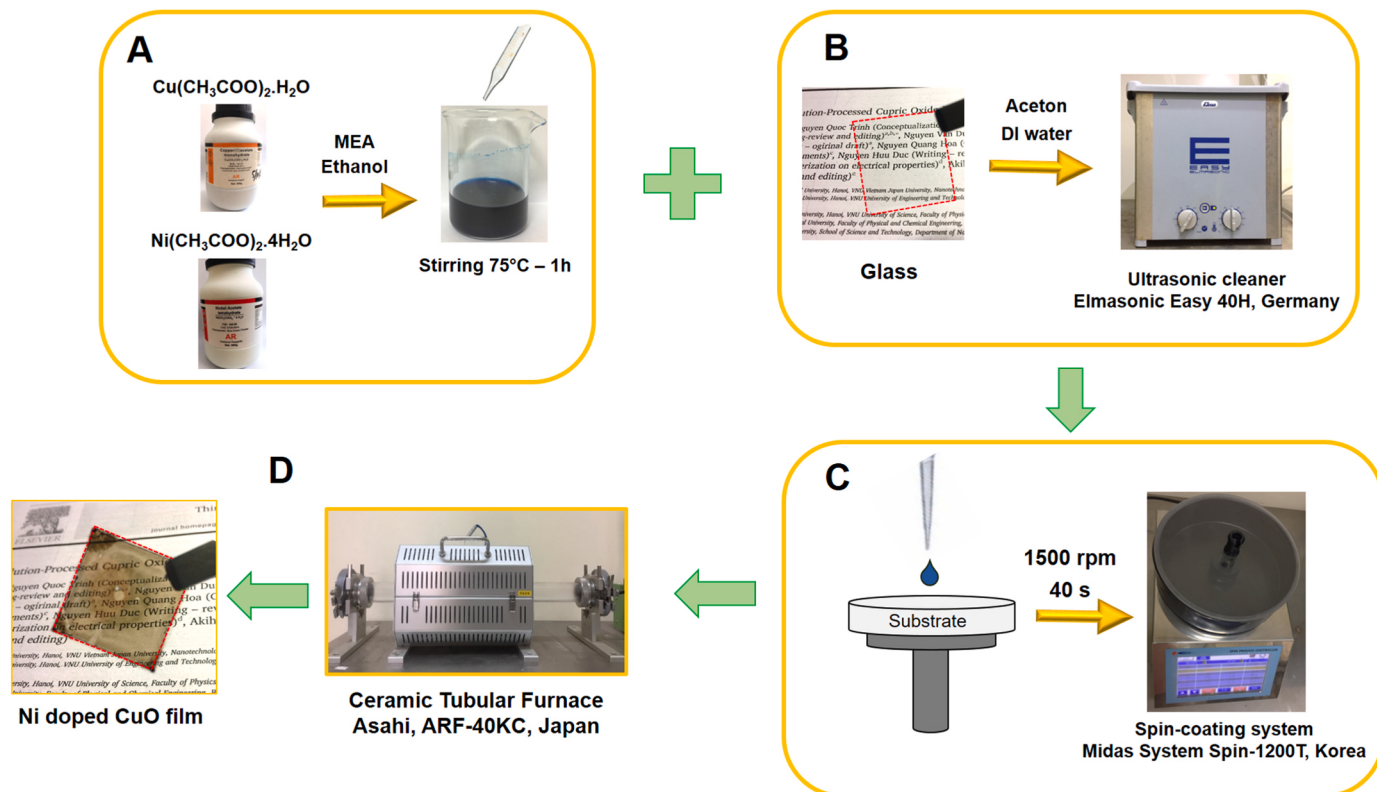


Fig. 1. Schematic drawing of the four stages: (A) preparing precursors, (B) cleaning substrates, (C) depositing the films, and (D) crystallizing the films.

coated by using a spin-coater (Midas System Spin-1200 T, Korea), and the spinning program was installed according to the procedures shown in Fig. 2. The stages in the spin-coating system that were installed correspond to the stages of film formation, including deposition, spin-up, spin-off, and evaporation steps. Specifically, in the spin-off phase, the Ni-CuO films were rotated at 1500 rpm for the 40 s to keep stable thickness. In this phase, the excess precursor solution flows to the edge and leaves as a droplet because the centrifugal force is greater than the viscous forces. In our previous work, we determined the thickness of films from a cross-sectional SEM observation [18]. Hence, in this work, we prepared all precursors with the same concentration of 0.25 M, spin-coated with the same program, and annealed with the same temperature. By this, we assume the thickness of films will not be much different from each other. Therefore, when changing the concentration ratio of Ni, the film-forming process of Ni-doped CuO films also were repeated three times so that the effect of Ni on the CuO film can be studied systematically. Finally, the films were annealed at 500 °C for 30 min in a furnace to obtain a crystalline structure as in the stage D.

## 2.2. Thin-film characterization and calculating method

Once the films were prepared via the deposition route as described above, they were characterized using X-ray diffraction (XRD), scanning electron microscopy (SEM), UV-Vis spectroscopy, and four-probe measurement. In detail, we determined the phase and the crystallinity of the films by using Bruker model D2 diffractometer, with Cu-K $\alpha$  radiation in the scanning range of 20°–80°. We observed the surface morphology of films by using SEM (Jeol, JSM-IT100). The sheet resistance of the films was evaluated at room temperature for each percentage of Ni doping using a four-probe measurement. The optical absorbance of films was measured by Shimadzu UV 2450-PC dual beam spectrophotometer, in the range of wavelengths from 300 to 800 nm. Based on the absorbance data, the absorption coefficient  $\alpha$  can be determined by the Beer-Lambert law, in which  $A$  is the absorbance and  $d$  is the film thickness.

$$\alpha = \frac{A}{d} \quad (1)$$

In the direct transitional gap materials, the optical bandgap energy,  $E_g$ , was extracted from the dependence of the absorption coefficient on the incident photon energy ( $h\nu$ ). The Tauc plot was used as follows [19]:

$$(\alpha h\nu) = C(h\nu - E_g)^{1/2} \quad (2)$$

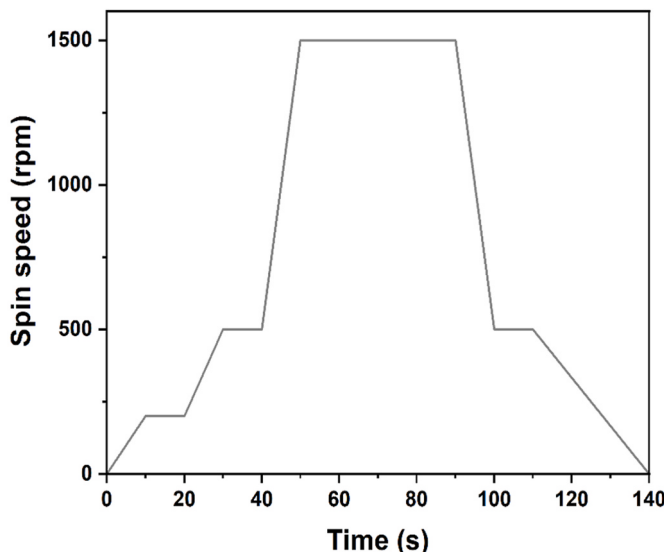


Fig. 2. Spin-coating program to keep stable the film thickness.

Where  $C$  is an energy-independent constant related to the material. Besides, the absorption coefficient is inversely proportional to the absorption length. In order to evaluate the absorption ability of films with the solar spectrum, the absorption length was normalized through the integral function, by the following equation [20,21]:

$$\frac{1}{L_a} = \frac{\int_{E_g}^{\infty} \alpha(E) u_{ph}(E) dE}{\int_{E_g}^{\infty} u_{ph}(E) dE} \quad (3)$$

Where  $\alpha(E)$  is the absorption coefficient as a function of the photon energy and  $u_{ph}$  is photon flux. Importantly, the key meaning of integral is to determine the area of any curves. Eq. (3) shows the relationship between the area of the absorption coefficient of the films and the area of the solar spectrum. The value of the absorption length can be determined in this relation, by applying the Riemann sum method. According to Fig. 3, the mathematical function is the blue line  $f(x)$ . The area under the curve is the integral of  $f(x)$  between the limits  $a$  and  $b$ , which is the integrated function between  $x = b$  and  $x = a$ . Then, the total area is calculated basing on the sum of small rectangles.

Assuming that the area of the small rectangle is  $A_i$  for the  $i^{\text{th}}$  rectangle, with  $\Delta x = x_{i+1} - x_i$ , and it can be expressed by:

$$A_i = \frac{y_{i+1} - y_i}{2} \times \Delta x \quad (4)$$

The total area of the curve is:

$$\text{Area} = \sum_{i=1}^n A_i \quad (5)$$

From Eqs. (4) and (5), the integral of the function between the absorption coefficient and the photon flux can be derived from a numerical method, and Eq. (3) turns into an approximation:

$$\frac{1}{L_a} = \frac{\int_{E_g}^{\infty} \alpha(E) u_{ph}(E) dE}{\int_{E_g}^{\infty} u_{ph}(E) dE} \approx \frac{\sum_{i=1}^n \alpha_i * u_i * \Delta E}{\sum_{i=1}^n u_i * \Delta E} = \frac{\sum_{i=1}^n \alpha_i * u_i}{\sum_{i=1}^n u_i} \quad (6)$$

## 3. Results and discussion

### 3.1. Structural analysis

The crystalline structure of Ni-doped CuO thin films with various Ni doping is shown in Fig. 4. It can be seen that the Ni-doped and un-doped CuO films were grown on glass substrates with high crystallinity. The peak positions observed at 34.75° and 37.73° correspond to the (002)

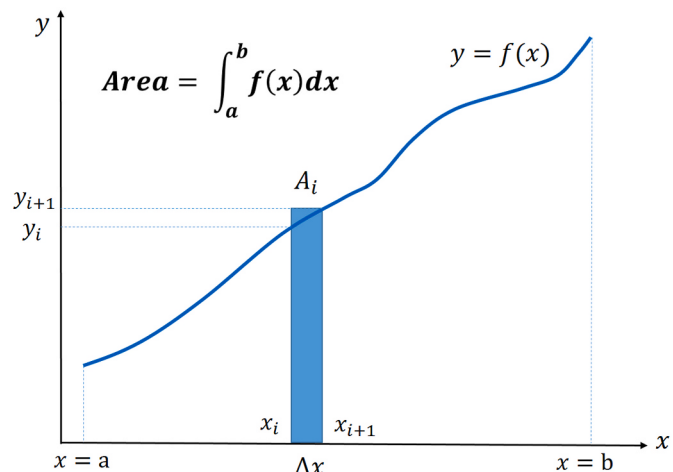


Fig. 3. The numerical way to calculate the total area of any function, known as the integral definition.

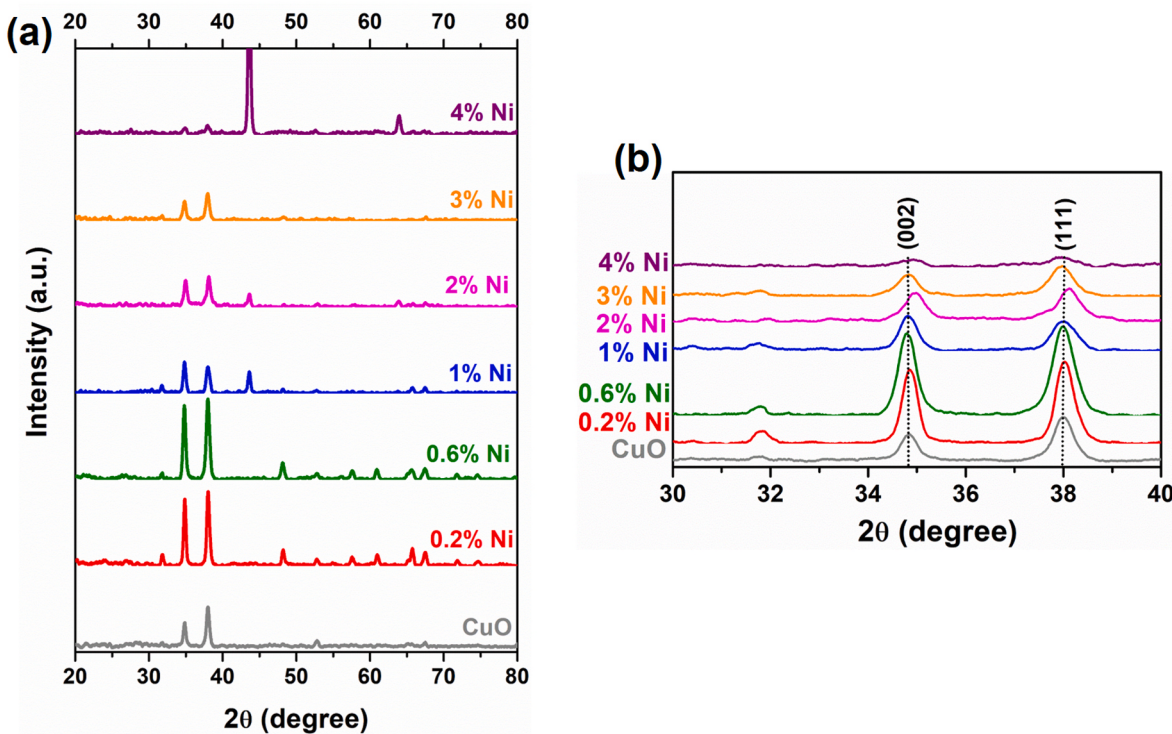


Fig. 4. XRD patterns of Ni-doped and un-doped CuO thin films (a), and the enlarged plot in the range of 30°–40° (b).

and (111) planes of CuO phase. The (002) and (111) peaks have considerably increased intensities than the other peaks, which indicated as preferred orientations and polycrystalline structure of the films. The preferably oriented peaks were in a matching agreement with our previous study [18]. In addition, no peaks related to the other common phase of  $\text{Cu}_2\text{O}$  can be detected in Fig. 4a, evidencing the films fabricated were only a single phase of CuO.

When Ni ions were introduced into the CuO base at doping lower than 1 wt%, specifically 0.2 and 0.6 wt% Ni, no peak of the NiO phase appeared and the film has a different crystal structure. However, a peak shift of (200) and (111) was observed in Fig. 4b. That is, Ni doping took place in part because Ni ions changed the lattice constants when they

entered the CuO matrix. The XRD patterns evidenced the presence of the NiO phase, and apparently, the intensity of the mainly oriented planes of the CuO phase gradually decreased as the Ni doping increased higher than 1 wt% (i.e. 2, 3, and 4 wt% Ni). The (200) and (020) orientations of NiO phases were detected at 43.41° and 65.61° positions as in Fig. 4a. When Ni ions were added to 4 wt%, the orientations of NiO (200) and (020) showed sharper peaks and were more obvious. This might indicate that below 1 wt% Ni concentration, Ni ions tend to intercalate or enter the holes of Cu ions. Meanwhile, at higher Ni concentrations, Ni ions has impacted the crystalline structure of CuO. From the result of Fig. 4, we can convince that the Ni-doped CuO films tended to form a composite structure when the Ni doping was higher than 1 wt%, leading to

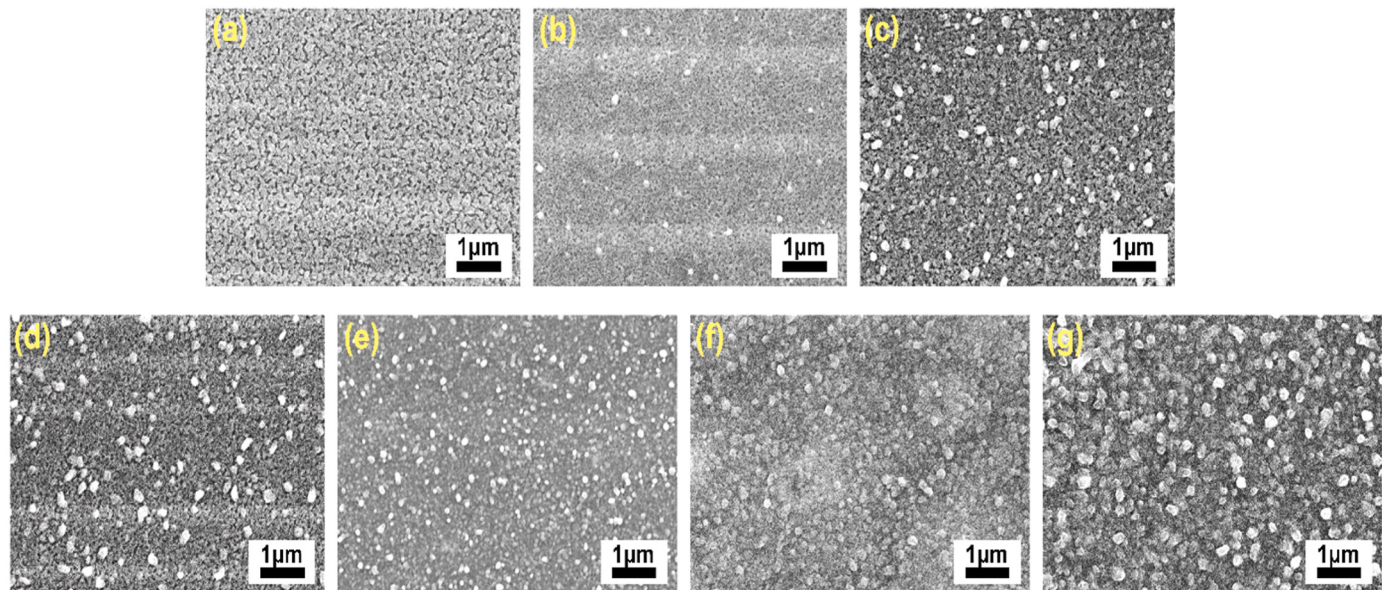


Fig. 5. SEM micrographs of Ni-doped CuO with Ni doping concentrations: (a) 0 wt%, (b) 0.2 wt%, (c) 0.6 wt%, (d) 1 wt%, (e) 2 wt%, (f) 3 wt%, and (g) 4 wt%.

interesting applications from a viewpoint of composite material.

### 3.2. Morphological analysis

The surface morphology of CuO films was observed by SEM and shown in Fig. 5. The SEM micrographs of the un-doped CuO film in Fig. 5a was relatively smooth with a flat surface. The observation was well-matched with our previous reports [18,22]. When the Ni ions were given into CuO-based films, distinct nanoparticles appeared on the surface of the films. In addition, nanoparticles became denser as the Ni doping increased, as observed from Fig. 5b to g. This result is consistent with the XRD analysis, for which the NiO phase developed when the Ni doping was higher due to the formation of the NiO particles on the surface. Our obtained data are similar to the research of Baturay et al. [23] of which they indicated that the coverage ratio of nanoparticles increased with Ni doping when Ni-doped CuO films were prepared by sol-gel method.

It can be also seen from Fig. 5 that, when the Ni doping concentration increased by 3 and 4 wt%, the inter-particle gap was filled, which could improve the electrical conductivity of the films. It is obvious that the appearance of nanoparticles assisted the films in expanding their ability to absorb and harvest more lights than the single CuO flat film, because of the roughness of nanoparticles. Here, for the different shapes of nanoparticles, the films will contain a scattering effect when light hits the film. It means that the nanoparticles on the film surface can distribute to the light capture, reduce the ability to reflect, and then increase the path of light [24,25].

To confirm the presence of Ni ions in the synthesized thin film CuO, EDS measurements were carried out as shown in Fig. 6. The two typical EDS spectra of CuO and 4% Ni–CuO films show a rather high percentage of elemental oxygen, due to the film heating process at high-temperature and a relatively long time. In addition, elements such as K, Si, Ti, Na, and Al from the composition of the glass substrate are observed, since the film is irradiated by a high-energy electron beam that can penetrate the film and interact with the substance in glass. Based on the Cu ratio obtained from the EDS, the Ni ratio was determined according to the following formula:

$$\%Ni_x = \frac{\%Cu_{EDS} \times \%Ni_0}{\%Cu_0}, \quad (7)$$

where,  $\%Ni_x$  is a theoretical-weight percent of Ni,  $\%Cu_{EDS}$  is a weight percent of the Cu element obtained by the EDS measurement,  $\%Ni_0$  is a weight percent of the initial Ni added during precursor synthesis, that is, 0.2, 0.6, 1, 2, 3, and 4 wt%, and  $\%Cu_0$  is a weight percent of the initial Cu, which is 99.8, 99.4, 99.98, and 97.96 wt%.

Table 1 shows the weight percent of Cu and Ni elements obtained from theoretical composition of Ni in proportion to Cu and EDS

**Table 1**

Weight percent of Cu and Ni elements obtained from theoretical composition of Ni in proportion to Cu and EDS measurement.

Samples	Weight percent of Cu (wt.%)	Weight percent of Ni (wt.%)		Ni/Cu ratio		
		Theory	Experiment	Theory	Experiment	
CuO	1.98	—	—	—	—	
0.2 wt%	0.48	0.001	0	0.002	0	
Ni–CuO	0.6 wt%	0.55	0.003	0	0.005	0
1 wt%	1.17	0.012	0.02	0.01	0.017	
Ni–CuO	2 wt%	8.63	0.176	0.14	0.02	0.016
3 wt%	1.09	0.034	0.02	0.031	0.018	
Ni–CuO	4 wt%	3.15	0.131	0.13	0.042	0.041

measurement. We can see that the Ni/Cu ratio in the samples was different from the initial Ni/Cu ratio for the cases of 0.2%, 0.6%, 1%, 2%, and 3%, except for the case of 4 wt% Ni doping film. This may be because the amount of Ni ions used is relatively small, so the distribution of Ni ions in the CuO film is not uniform, leading to differences in experimental and theoretical calculations. We believe that further investigation on the EDS spectroscopy needed to perform for an in-depth understanding this assumption in future.

### 3.3. Optical property

The optical property of the Ni-doped and un-doped CuO films was measured to evaluate the influence of Ni doping on the bandgap energy and the optical absorption from Fig. 7, in which a plot of optical absorbance spectra of the films as a function of Ni doping in the wavelength range of 300–800 nm is shown in Fig. 7a. No other peaks were observed in the UV–Vis region as all thin films were clear and uniform. It can be found from Fig. 7a that the absorbance increased with increasing the doping concentration, whereby the films with 4 wt% Ni doping had the highest absorbance. The increasing value of absorption with higher doping can be attributed to the expanded scattering of photons by crystal defects generated [23]. This result is related to the surface morphology of the films observed in Fig. 5, that is, the formation of nanoparticles on the surface extended the ability to capture more lights. Especially, when the density of nanoparticles was high, the absorption ability of the NIR region was enhanced [26].

Fig. 8 illustrates specifically the light absorption mechanism of CuO films and the surface plasmon mechanism of nanoparticles. For the pure CuO film, the absorption mechanism of the film is highly dependent on

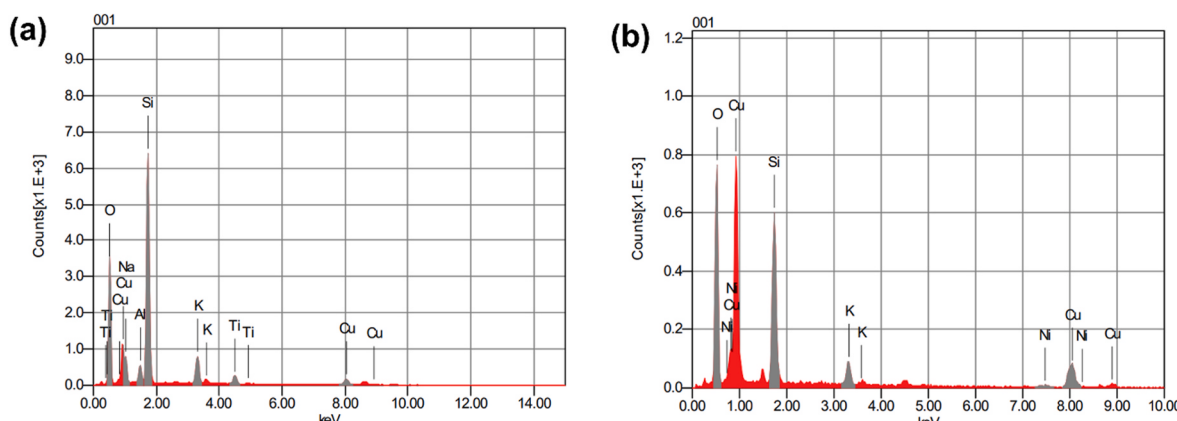


Fig. 6. EDS spectra of CuO (a) and 4 wt% Ni-doped CuO (b) samples.

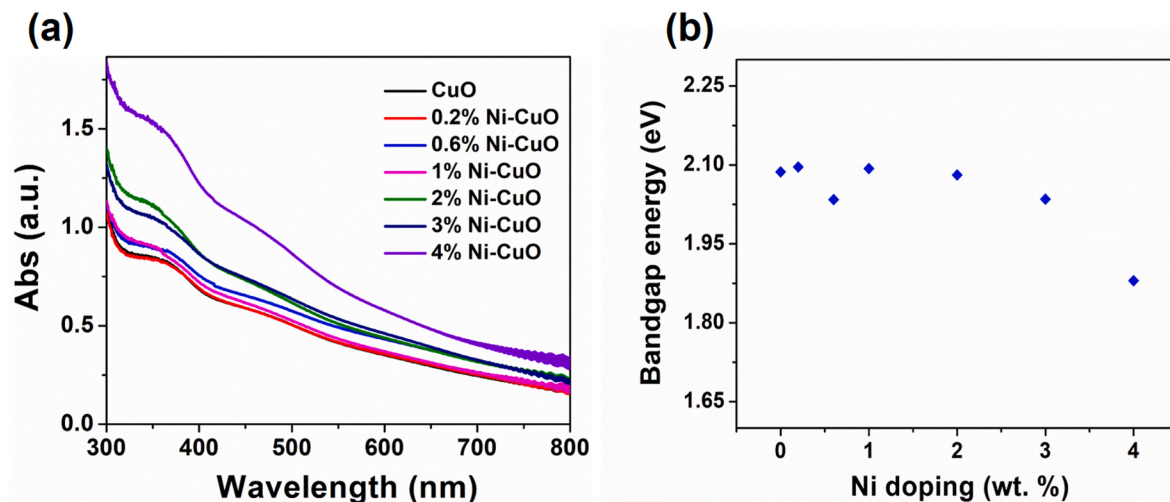


Fig. 7. Optical absorbance spectra (a), and bandgap energy values (b) for the Ni-doped and un-doped CuO thin films.

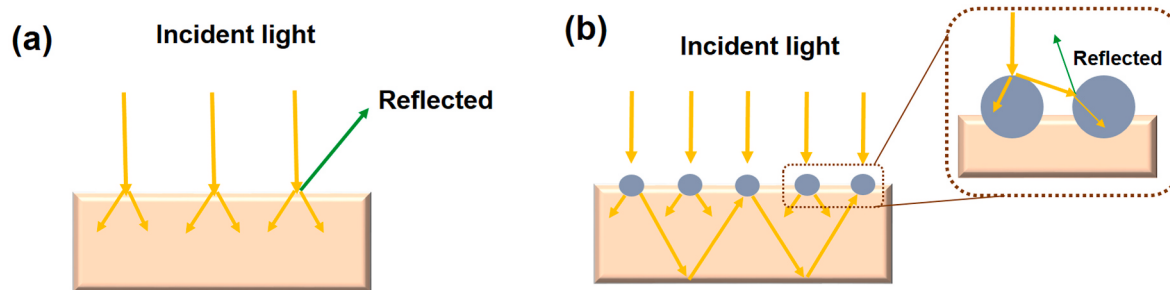


Fig. 8. Schematic drawing of the optical absorption mechanism for: a flat surface of the pure CuO films (a), and a surface plasmon resonance mechanism of Ni-doped CuO films (b).

the nature of films such as bandgap energy, the colour of films or the surface morphology of films. CuO is well-known as a narrow bandgap semiconductor [8] so that, the higher energy region of light is significantly transmitted out. Furthermore, when observing the SEM micrographs, it can be seen that the surface of the CuO film was relatively smooth and flat, which leads to an inefficient light capture due to high incident light reflection [27], as sketched in Fig. 8a. Therefore, it is essential to employ a technique that bolsters the absorption or trapping of light to enhance the path length of light and long-wavelength photons. Taking the presence of nanoparticles on the surface as an example, as shown in Fig. 8b, this architecture expanded light trapping using surface roughness [28]. Furthermore, the surface plasmon effect increased the effective path length without the need for overly thick absorbing films to scatter light into the thin film [24,29]. It means that the thickness of the thin absorption layer can reduce the recombination of the carriers and improve the energy conversion efficiency thanks to the plasmon structure [30]. The enhancement of light penetration into semiconductor thin films by scattering from plasmonic nanoparticles results in incident light passing through the semiconductor film several times and increasing the effective path length. In the absence of nanoparticles, long-wavelength photons can be reflected before being absorbed or transmitted and out through the film during absorption. The surface scattering of nanoparticles is a good step forward to extend light absorption in the NIR region of thin film materials that may be due to the plasmon resonance of the metal nanoparticles on the CuO planar surface [31–33].

The optical bandgap energy of the CuO-based films was estimated from their optical absorption characteristics. The Ni-doped and un-doped CuO films are a type of allowed direct transition gap materials. The bandgap energy compared with the Ni doping concentrations in the

grown thin films was plotted in Fig. 7b. The pure CuO film with the bandgap of 2.09 eV is the same as our previous work [18], and matched with the other research on CuO exhibited *p*-type conductivity and bandgap energy of 1.2–2.1 eV [34]. We obtained that the bandgap energy of the Ni-doped CuO films was 2.10, 2.03, 2.09, 2.08, 2.04, and 1.88 eV for 0.2, 0.6, 1, 2, 3, and 4 wt% doped CuO thin films, respectively. It was found that the bandgap energy decreased slightly as the Ni concentration increased from 0 to 4 wt %. This is because the concentration of Ni ions was still very small compared to the original CuO-based films, so the  $E_g$  changing between the Ni-doped and un-doped CuO films had not yet been significantly different. However, when the Ni doping increased to 4 wt%, the bandgap energy was dropped to 1.88 eV. It can be explained that the bandgap energy decreased because the impurity atoms added the ionization energy levels to the bandgap region. The scattering process of conduction electrons will be increased when the field inside the crystal is oscillated due to the existence of a high impurity concentration.

### 3.4. Electrical property

The variation of sheet resistance for the Ni-doped and un-doped CuO based films was obtained using a four-probe measurement. The values obtained for the sheet resistance at each concentration are shown in Table 2. The electrical property of films was affected by Ni doping. For the un-doped and 0.2 wt% Ni-doped CuO films, the sheet resistance was increased from 16.14 to 19.18 MΩ/sq and then decreased to 2.07 MΩ/sq, when the Ni doping concentration increased to 4 wt%. This result is consistent with the study of Baturay et al. [23], who reported that the film resistivity increased from  $2.35 \times 10^2$  to  $2.58 \times 10^2$  Ωcm for the case of 2% Ni doping. Also, they showed that the change in film resistivity

**Table 2**

Bandgap energy, sheet resistance, absorption length and absorption figure of merit for the CuO-based films with various Ni doping.

Ni doping (%)	$E_g$ (eV)	Sheet resistance ( $M\Omega/\text{sq}$ )	Absorption length (nm)	$a\text{-FOM}$ ( $\Omega^{-1}\text{cm}^{-1}$ )
0	2.09	16.14	99.93	6.19
0.2	2.10	19.18	99.49	5.19
0.6	2.03	9.45	90.40	9.57
1	2.09	9.31	95.10	10.21
2	2.08	4.94	80.18	16.23
3	2.04	6.44	80.74	12.53
4	1.88	2.07	63.80	30.82

from Ni doping could be due to the difference in the stoichiometric change caused by more Cu ion vacancies and electrically neutral defects in the surface of films. When Ni was further doped, the thin film simultaneously displayed the p-type [35] and magnetic properties of the Ni ions, providing better current control and electrical conductivity.

### 3.5. Analysis on the absorption figure of merit

Fig. 9 depicts the solar spectrum and absorption of Ni-doped CuO films in the range of 300–800 nm at various Ni ion ratios. For photovoltaic performance evaluation, the American Society for Testing and Materials provided solar absorption spectra, hence, we used it for this study. It is obvious that most of the solar spectrum has high intensity in the 400–800 nm spectral range, but CuO films have poor absorption in this region. However, when the Ni concentration was increased to 4 wt% doping, the doped Ni films exhibited a substantially better absorption ability in the UV–Vis wavelength range than that of CuO film. One of the reasons is that the nanoparticles on the Ni-doped film enhanced the absorption ability in the high absorptive region of the sun.

To compare the effectiveness of conductive films produced by different processes, the relationship between the optical absorption coefficient and the electrical conductivity was evaluated via the figure of merit [36]. The relationship is a method for correlating the properties of thin films constructed according to the formula of refs. [5,7].

$$F = (-\rho \ln T)^{-1} = (\rho ad)^{-1} \quad (8)$$

where  $\rho$  is the resistivity,  $T$  is the transmittance,  $\alpha$  is the absorption coefficient and  $d$  is the thickness of the film.

Ideally, the film with high absorption bolsters the effective conversion of light to electrical energy, while high conductivity facilitates the movement of fast electrons. However, if the internal resistance of films is

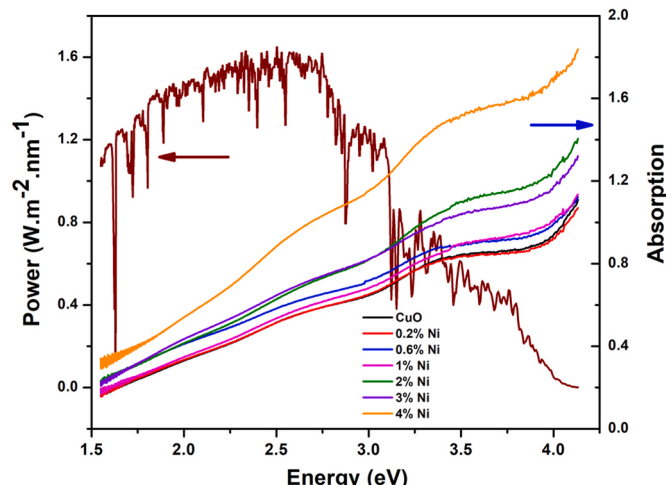


Fig. 9. Solar spectrum and absorbance of the Ni-doped CuO films in the wavelength region of 400–800 nm.

high, electrons will be hindered and difficult to travel. After that, when the  $p$ - $n$  junction is formed, the amount of captured light is turned into thermal energy, resulting in low power output for the films. Therefore, it is essential to define the fabricated film with good absorption at which wavelength regions for the solar spectrum in order to optimize that absorption and reduce the transmission of light. But, to our knowledge, no report that compares the solar spectrum to understand the nature of the experimental film. Thus, it is necessary to further evaluate the absorption of the film against the solar spectrum through the absorption length  $L_a$  as determined by Eq. (3).

The absorption length is given by the inverse of the absorption coefficient and it describes how deeply light can penetrate into a semiconductor material before being fully absorbed. At this point, the light has not yet implemented the absorption process to generate the minority and majority carriers. When light strikes a thin film, the portion of it is reflected back, while the rest that enters is absorbed or left the film. The absorption ( $A$ ) and transmission ( $T$ ) at each wavelength entering the film are  $A + T = 1 - R$ , where  $R$  is the reflectance [37]. Understandably, the absorption length describes the ability of photons to be trapped or left the material, and it is different from the moving path by the photon. Fig. 10a shows the values of  $L_a$  for the Ni-doped CuO film at various doping concentrations. The  $L_a$  value of pure CuO film was 99.93 nm, while the Ni-doped CuO films had a decreasing  $L_a$  value. In particular, the films with 0.2, 0.6, 1, 2, 3, 4 wt% Ni doping reached 99.49, 90.40, 95.10, 80.18, 80.74, and 63.80 nm, respectively. The  $L_a$  value of CuO was identical to those obtained by our published paper ( $L_a = 99$  nm) [18]. The presence of Ni ions modified the absorption length of the CuO film, resulting in an increase in the light absorption capacity of films. This is related to the energy of the photons, which is important for determining whether a photon is absorbed or transmitted. Because when the photon energy  $E_{ph}$  is less than the bandgap energy  $E_g$ , the light photons interact with the semiconductor weakly and pass through the film as if it were transparent.

In order to understand in-depth the absorptivity of films in comparison to the solar flux, the absorption figure of merit,  $a\text{-FOM}$  is introduced as mentioned above. This factor has been originally proposed by our group to evaluate the performance of CuO films in relation to the solar spectrum for solar cell applications [18]. The combination of the  $a\text{-FOM}$  factor and the absorption length is extremely advantageous for the absorption layer of materials with dark surfaces.

$$a\text{-FOM} = (\rho ad)^{-1} = \left( \frac{\int_{E_g}^{\infty} \alpha(E) u_{ph}(E) dE}{\int_{E_g}^{\infty} u_{ph}(E) dE} \right)^{-1} = \left( \rho d \frac{1}{L_a} \right)^{-1} = \frac{L_a}{\rho d} \quad (9)$$

The  $a\text{-FOM}$  was calculated by using Eq. (9), with Ni ion ratios of 0, 0.2, 0.6, 1, 2, 3, 4 wt% obtained at 6.19, 5.19, 9.57, 10.21, 16.23, 12.53, 30.88  $\Omega^{-1}\text{cm}^{-1}$ , respectively, as shown in Fig. 10b. The effect of resistivity and absorption length with Ni doping caused an increase in  $a\text{-FOM}$ , except for the case of 3 wt% Ni doping which had a slight decrease. Overall, Ni also had a positive effect on the process of absorbing energy from the sun. That is, the Ni-doped CuO films enhanced the light-harvesting performance of the solar spectrum and delivered power with low inherent resistance. The decrease in the absorption length is related to the increase in the diffusion length of the photons and leads to an increase in the absorption quality. Moreover, the lower the intrinsic resistance of the films not only increases the transport process but also reduces the light energy into heat. Therefore, the  $a\text{-FOM}$  is one of the important parameters to evaluate the photo-electrical characteristics of the absorbing materials when compared to the solar flux, as evidenced from this study.

### 4. Conclusion

We investigated the effect of Ni doping with 0.2, 0.6, 1, 2, 3, 4 wt% for the CuO-based films. The films were highly oriented along with (002) and (111) planes, according to the XRD patterns. We found that the

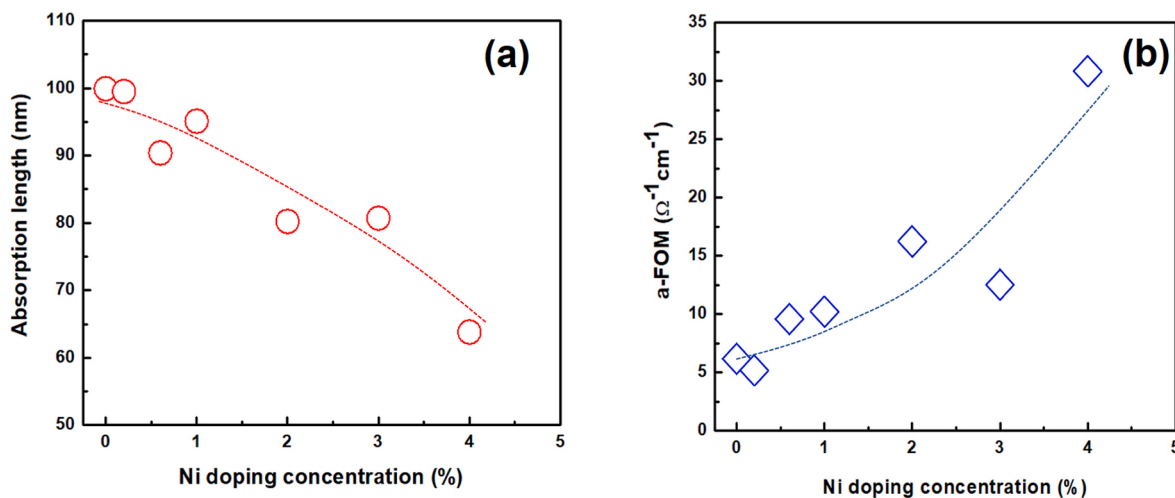


**Fig. 10.** Dependence of the absorption length (a) and the absorption figure of merit (b) on Ni doping concentration for the CuO-based films.

increase of Ni doping formed the NiO phase in the crystal structure of the films. A transformation of the surface morphology from a flat surface to an agglomeration of nanoparticles on the films, and the density of nanoparticles increased with the Ni doping concentration, were observed from SEM micrographs. The bandgap energy decreased from 2.09 to 1.88 eV when introducing a trace amount of Ni, and it makes the potential of the film in photovoltaic applications. The resistivity of the films improved from 16.14 M $\Omega$ /sq to 2.07 M $\Omega$ /sq for the Ni doping process. The combination of low resistivity and high optical absorption showed an improved absorption figure of merit, whose highest value of  $30.88 \Omega^{-1} \text{cm}^{-1}$  for the case of 4 wt% doping can be obtained, corresponding to the absorption length of 63.80 nm. Consequently, this achievement will bring an important way to characterize the films prior to determining the solar spectrum applicability of any conductive oxide semiconductor materials in photonic devices.

#### CRediT authorship contribution statement

**Nguyen Van Loi:** Samples Preparation, Investigation, Writing – original draft. **La Thi Ngoc Mai:** Samples Preparation, Formal analysis, Validation, Investigation, Writing – original draft. **Nguyen Hoang Luong:** Writing – review & editing. **Bui Nguyen Quoc Trinh:** Conceptualization, Methodology, Formal analysis, Validation, Writing – original draft, Writing – review & editing.

#### Declaration of competing interest

The authors declare that they have no known competing financial interests or personal relationships that could have appeared to influence the work reported in this paper.

#### Data availability

Data will be made available on request.

#### Acknowledgments

This work is fully supported by the project with the code number of VJU. JICA.21.03, from Vietnam Japan University, under Research Grant Program of Japan International Cooperation Agency, Japan.

#### References

- [1] F.E. Subhan, A.D. Khan, F.E. Hilal, A.D. Khan, S.D. Khan, R. Ullah, M. Imran, M. Noman, Efficient broadband light absorption in thin-film a-Si solar cell based on double sided hybrid bi-metallic nanogratings, RSC Adv. 10 (2020) 11836–11842, <https://doi.org/10.1039/C9RA.10232A>.
- [2] S. Eyderman, A. Deinega, S. John, Near perfect solar absorption in ultra-thin-film GaAs photonic crystals, J. Mater. Chem. 2 (2014) 761–769.
- [3] S. Yu, W. Zhang, L. Li, D. Xu, H. Dong, Y. Jin, Optimization of SnO<sub>2</sub>/Ag/SnO<sub>2</sub> tri-layer films for enhanced composite electrode with high figure of merit, Thin Solid Films 552 (2014) 150–154, <https://doi.org/10.1016/j.tsf.2013.11.109>.
- [4] J. Ho Kim, Y.-J. Moon, S.-K. Kim, Y.-Z. Yoo, T.-Y. Seong, Al-doped ZnO/Ag-Al-doped ZnO multilayer films with a high figure of merit, Ceram. Int. 41 (2015) 14805–14810.
- [5] S. Velusamy, P. Vickraman, Annealing temperature dependent on structural, optical and electrical properties of indium oxide thin films deposited by electron beam evaporation method, Curr. Appl. Phys. 10 (2010) 880–885.
- [6] A.M. El Sayed, Exploring the morphology, optical and electrical properties of nickel oxide thin films under lead and iridium doping, Phys. B 600 (2021), 412601, <https://doi.org/10.1016/j.physb.2020.412601>.
- [7] S. Cho, Optical and electrical properties of CuO thin films deposited at several growth temperatures by reactive RF magnetron sputtering, Met. Mater. Int. 19 (2013) 1327–1331.
- [8] R. Sahay, J. Sundaramurthy, P. Suresh Kumar, V. Thavasi, S.G. Mhaisalkar, S. Ramakrishna, Synthesis and characterization of CuO nanofibers, and investigation for its suitability as blocking layer in ZnO NPs-based dye sensitized solar cell and as photocatalyst in organic dye degradation, J. Solid State Chem. 186 (2012) 261–267, <https://doi.org/10.1016/j.jssc.2011.12.013>.
- [9] M.-Y. Lin, C.-Y. Lee, S.-C. Shiu, I.-J. Wang, J.-Y. Sun, W.-H. Wu, Y.-H. Lin, J.-S. Huang, C.-F. Lin, Sol-gel processed CuOx thin film as an anode interlayer for inverted polymer solar cells, Org. Electron. 11 (2010) 1828–1834.
- [10] S. Karthick Kumar, S. Suresh, S. Murugesan, S.P. Raj, CuO thin films made of nanofibers for solar selective absorber applications, Sol. Energy 94 (2013) 299–304, <https://doi.org/10.1016/j.solener.2013.05.018>.
- [11] A.M. El Sayed, M. Shaban, Structural, optical and photocatalytic properties of Fe and (Co, Fe) co-doped copper oxide spin coated films, Spectrochim. Acta, Part A 149 (2015) 638–646.
- [12] M. Nesa, M. Sharmin, K.S. Hossain, A.H. Bhuiyan, Structural, morphological, optical and electrical properties of spray deposited zinc doped copper oxide thin films, J. Mater. Sci. Mater. Electron. 28 (2017) 12523–12534.
- [13] H. El Aakib, J.F. Pierson, M. Chaik, H. Ait Dads, C. Samba Vall, A. Narjis, A. Outzourhit, Nickel doped copper oxide thin films prepared by radiofrequency reactive sputtering: study of the impact of nickel content on the structural, optical and electrical properties, Spectrosc. Lett. 54 (2021) 487–494.
- [14] S. Baturay, A. Tombak, D. Batibay, Y.S. Ocak, n-Type conductivity of CuO thin films by metal doping, Appl. Surf. Sci. 477 (2019) 91–95.
- [15] A. Zeb, M. Arfan, T. Shahid, T.B. Masood, A.G. Wattoo, Z. Song, M. Shahzad, S. M. Ansari, Tailoring of pyramid cobalt doped nickel oxide nanostructures by composite-hydroxide-mediated approach, Mater. Chem. Phys. 239 (2020), 122036.
- [16] A. J., T. Sahoo, Effect of Li doping on conductivity and band gap of nickel oxide thin film deposited by spin coating technique, Mater. Res. Express 7 (2019), 016405.
- [17] M.N. Siddique, A. Ahmed, P. Tripathi, Dielectric relaxation and Hopping conduction mechanism in Ni<sub>1-x</sub>Cr<sub>x</sub>O nanostructures, Mater. Chem. Phys. 239 (2020), 121959.
- [18] H.Q. Nguyen, D. Van Nguyen, A. Fujiwara, B.N.Q. Trinh, Solution-processed CuO thin films with various Cu<sup>2+</sup> ion concentrations, Thin Solid Films 660 (2018) 819–823, <https://doi.org/10.1016/j.tsf.2018.03.036>.
- [19] S.S. Shariffudin, S.S. Khalid, N.M. Sahat, M.S.P. Sarah, H. Hashim, Preparation and characterization of nanostructured CuO thin films using sol-gel dip coating, IOP Conf. Ser. Mater. Sci. Eng. 99 (2015), 012007.
- [20] J.J. Loferski, Thin films and solar energy applications, Surf. Sci. 86 (1979) 424–443.

- [21] F. Alharbi, J.D. Bass, A. Salhi, A. Alyamani, H.-C. Kim, R.D. Miller, Abundant non-toxic materials for thin film solar cells: alternative to conventional materials, *Renew. Energy* 36 (2011) 2753–2758.
- [22] B.N.Q. Trinh, N. Van Dung, N.Q. Hoa, N.H. Duc, D.H. Minh, A. Fujiwara, Solution-processed cupric oxide P-type channel thin-film transistors, *Thin Solid Films* 704 (2020), 137991, <https://doi.org/10.1016/j.tsf.2020.137991>.
- [23] S. Baturay, A. Tombak, D. Kaya, Y.S. Ocak, M. Tokus, M. Aydemir, T. Kilicoglu, Modification of electrical and optical properties of CuO thin films by Ni doping, *J. Sol. Gel Sci. Technol.* 78 (2016) 422–429, <https://doi.org/10.1007/s10971-015-3953-4>.
- [24] H.A. Atwater, A. Polman, Plasmonics for improved photovoltaic devices, *Nat. Mater.* 9 (2010) 205–213.
- [25] K.R. Catchpole, A. Polman, Design principles for particle plasmon enhanced solar cells, *Appl. Phys. Lett.* 93 (2008), 191113.
- [26] S. Pillai, M.A. Green, Plasmonics for photovoltaic applications, *Sol. Energy Mater. Sol. Cells* 94 (2010) 1481–1486.
- [27] C. Niu, T. Zhu, Y. Lv, Influence of surface morphology on absorptivity of light-absorbing materials, *Int. J. Photoenergy* 2019 (2019), 1476217.
- [28] H.W. Deckman, C.B. Roxlo, E.J. O.I. Yablonovitch, Maximum statistical increase of optical absorption in textured semiconductor films, *Opt. Lett.* 8 9 (1983) 491–493.
- [29] P. Spinelli, V.E. Ferry, J. van de Groep, M. van Lare, M.A. Verschuur, R.E. I. Schropp, H.A. Atwater, A. Polman, Plasmonic light trapping in thin-film Si solar cells, *J. Opt.* 14 (2012), 024002, <https://doi.org/10.1088/2040-8978/14/2/024002>.
- [30] C. Fei Guo, T. Sun, F. Cao, Q. Liu, Z. Ren, Metallic nanostructures for light trapping in energy-harvesting devices, *Light Sci. Appl.* 3 (2014), <https://doi.org/10.1038/lsta.2014.42>, 161–161.
- [31] D. Derkacs, S.H. Lim, P. Matheu, W. Mar, E.T. Yu, Improved performance of amorphous silicon solar cells via scattering from surface plasmon polaritons in nearby metallic nanoparticles, *Appl. Phys. Lett.* 89 (2006), 093103.
- [32] F.J. Beck, A. Polman, K.R. Catchpole, Tunable light trapping for solar cells using localized surface plasmons, *J. Appl. Phys.* 105 (2009), 114310, <https://doi.org/10.1063/1.3140609>.
- [33] A.S.M. Mohsin, M. Mobashera, A. Malik, M. Rubaiat, M. Islam, Light trapping in thin-film solar cell to enhance the absorption efficiency using FDTD simulation, *J. Opt.* 49 (2020) 523–532, <https://doi.org/10.1007/s12596-020-00656-w>.
- [34] H. Siddiqui, M. Parra, P. Pandey, N. Singh, M. Qureshi, F. Haque, A review: synthesis, characterization and cell performance of Cu<sub>2</sub>O based material for solar cells, orient, *J. Chem.* 28 (2012) 1533–1545.
- [35] D. Wu, Q. Zhang, M. Tao, LSDA + U study of cupric oxide: electronic structure and native point defects, *Phys. Rev. B* 73 (2006), 235206.
- [36] V.K. Jain, A.P. Kulshreshtha, Indium-Tin-Oxide transparent conducting coatings on silicon solar cells and their “figure of merit”, *Sol. Energy Mater.* 4 (1981) 151–158.
- [37] D. Zhou, R. Biswas, Photonic crystal enhanced light-trapping in thin film solar cells, *J. Appl. Phys.* 103 (2008), 093102, <https://doi.org/10.1063/1.2908212>.